arXiv:cond-mat/0703789v2 [cond-mat.mes-hall] 30 Oct 2007

Enhancing the spin-transfer torque through proximity of quantum well states

Ioannis Theodonis,[1,2,*] Alan Kalitsov,[1] and Nicholas Kioussis[1]

[1]*Department of Physics, California State University, Northridge, CA 91330-8268*
[2]*Department of Physics, National Technical University, GR-15773, Zografou, Athens, Greece*

(Dated: February 6, 2008)

We predict that the spin-transfer, $T_{i,||}$, and field-like, $T_{i,\perp}$, components of the *local* spin torque are dramatically enhanced in double-barrier magnetic tunnel junctions. The *spin-mixing* enhancement is due to the energetic proximity of majority and minority quantum well states (QWS) of different quantum numbers within the bias window. $T_{i,||}$ exhibits a switch-on and switch-off step-like bias behavior when spin polarized QWS enter the bias window or exit the energy band, while $T_{i,\perp}$, changes sign between switch-on biases. The *net* $T_\perp$ exhibits an anomalous angular behavior due to the bias interplay of the bilinear and biquadratic effective exchange couplings.

PACS numbers: 85.75.-d, 72.10.-d, 72.25.-b, 73.40.Gk

I. INTRODUCTION

Spintronics involve the exploitation of the quantum-mechanical spin degree of freedom to provide new functionalities beyond conventional electronics[1]. One effect that has its roots on the electron's spin, is the torque exerted on the magnetization of a nanometer-scale free ferromagnet (FM) by a spin-polarized current, originating from a preceding non-collinear pinned FM[2, 3, 4]. This torque can be decomposed into a field-like and a spin-transfer component[5], both orthogonal to the magnetic moment of the free FM, but with different influence on its dynamics[6]. Recent ferromagnetic resonance experiments, provide a useful tool to study the role of each component[7, 8]. At sufficiently high current densities, the spin-transfer torque leads to current-induced magnetization switching (CIMS)[9, 10, 11]. Reduction of the high critical current for CIMS is necessary for spin-transfer controlled magnetic memories[12].

Double-barrier magnetic tunnel junctions (DBMTJ) consist of a central metallic layer between two insulating barriers and two FM electrodes. The tunneling magnetoresistance (TMR) can be dramatically enhanced in *collinear* DBMTJ by the presence of quantum well states (QWS) under appropriate resonant conditions[13, 14, 15, 16]. Recently, the discrete energy spectrum of FM nanoparticles has been shown to enhance spin accumulation and to control the bias dependence of the TMR[17]. While the physics in *collinear* DBMTJ has been studied extensively[13, 14, 15, 16], the effect of *spin-polarized* QWS (SPQWS) on the spin-torque in *non-collinear* DBMTJ remains an unexplored area thus far.

The objective of this work is to present for the first time a study of the effect of SPQWS on both the *spin-transfer* $T_{||}$ and *field-like* $T_\perp$ components of the spin torque under external bias. The calculations are based on the tight-binding method and the non-equilibrium Keldysh formalism. We predict that both components of the *local* spin torque can be dramatically enhanced when majority and minority QWS energies of different quantum numbers are in close proximity and lie within the bias window. It should be emphasized that the local-spin-torque enhancement is not associated with an enhancement of the corresponding spin-polarized currents. The low-temperature bias dependence of the local spin-transfer torque,$T_{i,||}$, exhibits a switch-on and switch-off step-like behavior when the SPQWS enter the bias window or exit the energy band, respectively, similar to that of the spin-polarized currents. On the other hand, $T_{i,\perp}$ changes sign between the majority and minority switch-on values of bias. We demonstrate that the bias behavior of $T_{i,||}$ and $T_{i,\perp}$ can be derived analytically using a single-site central FM region. The *net* $T_\perp$, pertinent to the non-equilibrium interlayer exchange coupling, E_{XC}, exhibits an anomalous angular behavior due to the interplay of the bilinear and biquadratic effective exchange couplings which have different bias behavior.

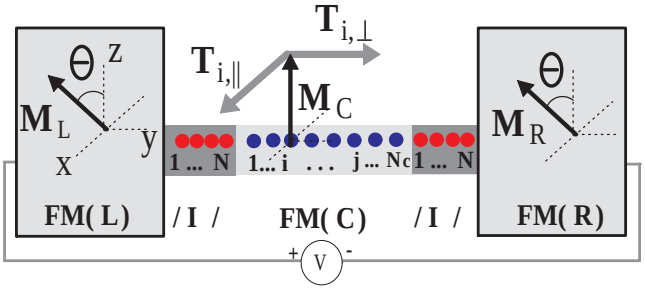

FIG. 1: (Color Online) Schematic of the DBMTJ consisting of a FM central wire of N_C atomic sites, connected to left and right FM leads through the tunneling barriers I of N sites. The spin-transfer (field-like), $T_{i,||}$ ($T_{i,\perp}$) components of the torque lies in the -x (y) directions.

The structure of this paper is as follows. In Sec. II, we introduce the basic model and outline the computational approach of the non-equilibrium spin torque. In Sec. III, we present and discuss the results of the calculations. Finally, Sec. IV includes a brief statement of the

*E-mail: ytheod@mail.ntua.gr

conclusions.

II. METHOD - FORMALISM

Fig.1 shows the one-dimensional FM/I/FM/I/FM DBMTJ system, consisting of a central (C) FM nanowire containing N_C atomic sites (AS) connected to the left (L) and right (R) FM electrodes through two thin symmetric non-magnetic tunneling barrier nanowires I of $N = 2$ AS. The magnetization of the central FM, $\mathbf{M}_C$, is along the z axis of the coordinate system shown in Fig. 1. The magnetization of the FM leads $\mathbf{M}_{L(R)}$ lies in the $x-z$ plane, i.e. it is rotated by angle θ around the wire axis y. The Hamiltonian of the system is

$$H = H_L + H_M + H_R + H_{L,M} + H_{R,M} + hc, \quad (1)$$

where $H_M = H_I + H_C + H_{I,C} + hc$ is the Hamiltonian of the middle (M) multi-layer I/FM/I region, and $H_{L(R),M}, H_{I,C}$ are the coupling Hamiltonians at the L(R)/M and I/C interfaces, respectively. The Hamiltonian for each FM region H_α, α= L, R, and C, is described by a one-dimensional single-orbital tight-binding model neglecting the in-plane k-dependence, which includes a nearest-neighbor (NN) spin-independent hopping term, t_α, and a spin-dependent on-site energy term, $\varepsilon_\alpha^\sigma$, i.e.,

$$H_\alpha = \sum_{\sigma,i} \varepsilon_\alpha^\sigma c_i^\dagger c_i + \sum_i t_\alpha c_i^\dagger c_{i+1} + hc. \quad (2)$$

The Hamiltonian, H_I, for the barriers is identical to H_α, but where one replaces the hopping term t_α with t_I and the spin-dependent on-site energy $\varepsilon_\alpha^\sigma$ with the spin-independent ε_I. The coupling Hamiltonian of the FM/I interface is $H_{\alpha,I} = t_{\alpha/I} c_\alpha^\dagger c_I$. The exchange-splitting, $\Delta_\alpha = \varepsilon_\alpha^\uparrow - \varepsilon_\alpha^\downarrow$, is identical in all FMs, $\Delta_{\rm I} = 0$, $\varepsilon_\alpha^\uparrow - E_F = 0.318$ eV, $\varepsilon_\alpha^\downarrow - E_F = 0.736$ eV, and $\varepsilon_{\rm I} - E_F = 6.5$ eV, where E_F is the Fermi energy. The $t_\alpha = 0.4$ eV in all FMs, $t_I = 1$ eV in both insulators, and $t_{\alpha/I} = 0.5$ eV in all FM/I interfaces, consistent with the *ab initio* values for 1D Co FM nanowires[18].

We extend Datta's formalism [19] to the case of non-collinear systems, where the scalar Green functions are replaced with 2x2 matrices in spin space. For this purpose, H_α can be expressed in the form, $H_\alpha = \bar{H}_\alpha + \delta H_\alpha$, where

$$\bar{H}_\alpha = \tfrac{1}{2}(\varepsilon_\alpha^\uparrow + \varepsilon_\alpha^\downarrow) + t_\alpha, \quad (3)$$

describes the spin-average part of H_α and

$$\delta H_\alpha = \tfrac{1}{2}(\varepsilon_\alpha^\uparrow - \varepsilon_\alpha^\downarrow) \quad (4)$$

is the spin-splitting part of H_α. The one-electron Schrödinger equation for the retarded Green function, $g_{pq}^{\sigma,\sigma'}$, in each isolated semi-infinite ferromagnetic lead becomes

$$\sum_{p_1} \left[(E\delta_{pp_1} - \bar{H}_{pp_1}) I - \delta H_{pp_1} \begin{pmatrix} cos\theta & sin\theta \\ sin\theta & -cos\theta \end{pmatrix} \right] \times \begin{pmatrix} g_{p_1q}^{\uparrow\uparrow} & g_{p_1q}^{\uparrow\downarrow} \\ g_{p_1q}^{\downarrow\uparrow} & g_{p_1q}^{\downarrow\downarrow} \end{pmatrix} = \delta_{pq} I, \quad (5)$$

where I is a 2x2 unit matrix. Following Datta [19] we find that the retarded Green function of the middle region M is

$$\hat{G}_M = [E\hat{I} - \hat{H}_M - \hat{\Sigma}_L - \hat{\Sigma}_R]^{-1}, \quad (6)$$

where E is the one-electron electron energy, $\hat{H}_M$ and $\hat{\Sigma}_{L(R)}$ are the $(2N_M \times 2N_M)$ Hamiltonian and self-energy matrices, respectively, and $N_M = 2N + N_C$ is the number of atomic sites in the middle region. The only non-zero elements of $\hat{\Sigma}_{L(R)}$ are the (2×2) self-energy matrices at the interfacial sites

$$\tilde{\Sigma}_{L(R)}(\theta) = t_{\alpha/I}^2 \tilde{g}_{L(R)}(\theta), \quad (7)$$

where $\tilde{g}_{L(R)}(\theta)$ are the retarded surface 2×2 Green's function matrices of the isolated L(R) lead, determined from Eq. 5. The non-equilibrium Green's functions can be determined by solving the kinetic equation [19]

$$\hat{G}_M^< = i\hat{G}_M \hat{\Sigma}^< \hat{G}_M^\dagger, \quad (8)$$

where $\hat{\Sigma}^< = f_L(\hat{\Sigma}_L^\dagger - \hat{\Sigma}_L) + f_R(\hat{\Sigma}_R^\dagger - \hat{\Sigma}_R)$, is the non-equilibrium self-energy matrix and $f_{L(R)}$ are the Fermi-Dirac distribution functions of the L(R) leads.

The local spin-transfer torque $\mathbf{T}_i$ exerted on the local moment at site i in the central FM region is[20]

$$\mathbf{T}_i \equiv -\nabla \cdot \boldsymbol{I}^{(s)} = \boldsymbol{I}_{i-1,i}^{(s)} - \boldsymbol{I}_{i,i+1}^{(s)}, \quad (9)$$

where

$$\boldsymbol{I}_{i,i\pm1}^{(s)} = \frac{t_C}{4\pi} \int Tr_\sigma \left[(\tilde{G}_{i,i\pm1}^< - \tilde{G}_{i\pm1,i}^<) \boldsymbol{\sigma} \right] dE, \quad (10)$$

is the spin current between NN sites[20], and $\boldsymbol{\sigma} = (\sigma_x, \sigma_y, \sigma_z)$ is a vector of the Pauli matrices. The field-like, $T_{i,\perp}$, and spin-transfer, $T_{i,\parallel}$, components of the local spin torque, shown in Fig. 1, are along the $\hat{M}_C \times (\hat{M}_{L(R)} \times \hat{M}_C)$ and $\hat{M}_C \times \hat{M}_{L(R)}$ directions, respectively. Here, $\hat{M}_C$ and $\hat{M}_{L(R)}$ are unit vectors along the magnetization of the free C and pinned L(R) FM regions, respectively.

III. RESULTS - DISCUSSION

The majority-(full triangles) and minority-(open triangles) QWS energies relative to the Fermi energy, E^{n^σ}, as a function of the thickness, N_C, of the central FM wire are shown in Fig. 2 for QWS between -0.5 eV and 0.5 eV. The numbers next to each series of data points,

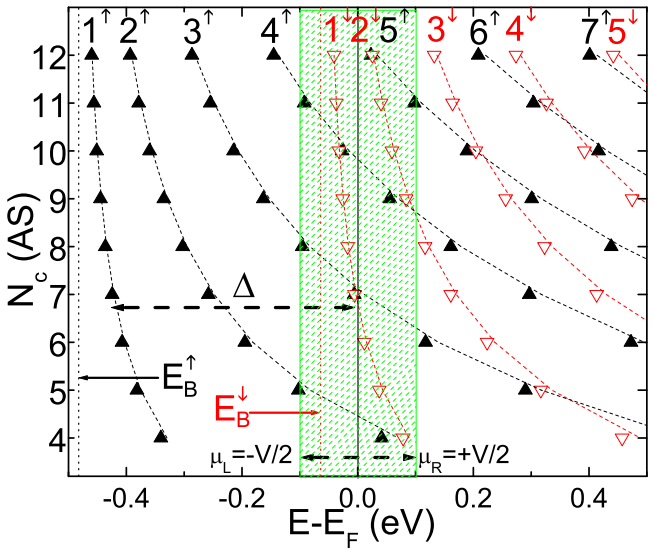

FIG. 2: (Color online) SPQWS energy positions E^{n^σ} as a function of the number of atomic sites, N_c, in the central FM region for zero bias and $\theta = 0$. The bottom of the majority (minority) conduction band of the leads is denoted by $E_B^{\uparrow(\downarrow)}$ and Δ is the exchange splitting, denoted by the dashed horizontal arrow. At finite bias V, the chemical potentials of the L,R leads are shifted by $eV = \mu_R - \mu_L$ around the Fermi energy.

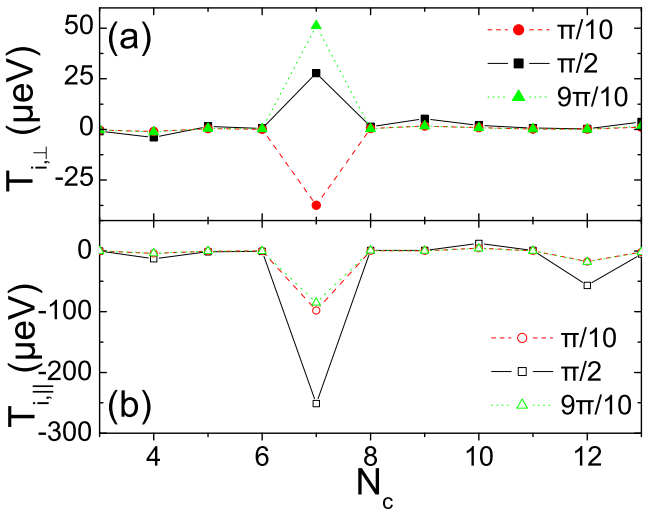

FIG. 3: (Color online) Low-temperature (T=5 K) and low-bias (V = 0.1 V) (a) perpendicular, $T_{i,\perp}$, and (b) parallel, $T_{i,||}$, components of the local spin torque versus the number of atomic sites, N_c, of the central FM region. Both components of the local spin torques are calculated on the first site in the central FM region next to the left FM/I interface for three values of the angle θ of $\pi/10$, $\pi/2$, and $9\pi/10$, respectively.

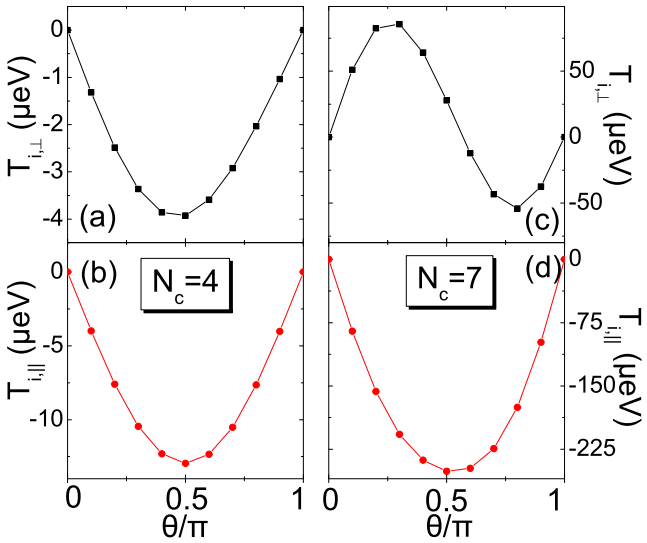

FIG. 4: (Color online) Angular dependence of $T_{i,\perp}$ (black squares) and $T_{i,||}$ (red circles) for $N_c = 4$AS in panels (a) and (b), and for $N_c = 7$AS in panels (c) and (d), respectively. The local spin torque is evaluated on the first site in the central FM region next to the left FM/I interface at $T = 5K$ and $V = 0.1V$.

indicate the quantum number, $n^\sigma = 1^\sigma, 2^\sigma, \ldots, N_c^\sigma$, of the SPQWS. The dashed curves denote the SPQWS energies, $E_0^{n^\sigma} = \varepsilon^\sigma + 2t\cos(n^\sigma\pi/(N_C+1))$ of the isolated central FM wire. The coupling of the central region to the FM leads results in a shift and a broadening of the SPQWS energies. The bottom of the majority (minority) conduction band of the leads, at zero bias, is indicated by $E_B^{\uparrow(\downarrow)}$. Note, that for $N_c = 7$AS the $n^\uparrow = 3^\uparrow$ majority- and $n^\downarrow = 1^\downarrow$ minority QWS are in very close proximity and they are very close to the Fermi energy. Under applied bias V, only the SPQWS with energies E^{n^σ} that lie within the bias window from $\mu_L = -\frac{eV}{2}$ to $\mu_R = +\frac{eV}{2}$, denoted by the shaded area in Fig. 2, contribute to the resonant tunneling.

In Figs. 3a and 3b we show the perpendicular, $T_{i,\perp}$, and parallel, $T_{i,||}$, components of the local spin torque on the first site ($i = 1$) in the central FM region next to the left FM/I interface, as a function of the thickness N_c of the central FM region. Both local spin torque components are calculated at T=5K and V=0.1V, for the almost parallel $\theta = \pi/10$, perpendicular $\theta = \pi/2$ and almost antiparallel $\theta = 9\pi/10$ configurations. We find that $T_{i,\perp}$ and $T_{i,||}$ are strongly enhanced for $N_c = 7$ AS by about one and two orders of magnitude, respectively. The local spin-torque enhancement persists even for very small angular deviations from the parallel(circles) and antiparallel(triangles) configurations. Interestingly, $T_{i,\perp}$ for $N_c = 7$ changes sign with increasing θ, in contrast to $T_{i,||}$.

In Figs. 4a,4c and 4b,4d we display the angular dependence of the perpendicular, $T_{i,\perp}$, (black squares) and parallel $T_{i,||}$ (red circles) components of the *local* spin torque for $N_c = 4$AS and $N_c = 7$AS, respectively. The spin torques are evaluated on the first site in the central FM region next to the left FM/I interface at T=5K and V=0.1V. In both cases (Figs. 4b and 4d) $T_{i,||}$, exhibits a sinusoidal angular dependence similar to that in a single

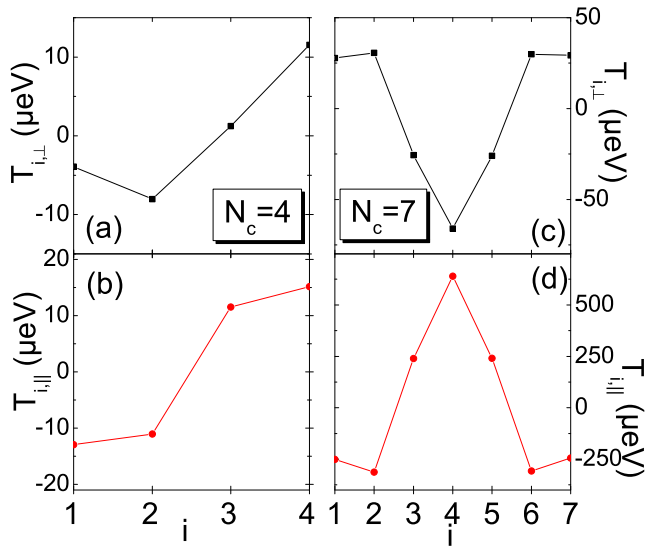

FIG. 5: (Color online) Perpendicular, $T_{i,\perp}$ (black squares, and parallel, $T_{i,||}$ (red circles), components of spin torque as a function of site i in the central FM region, for $N_c = 4$AS in panels (a) and (b) and for $N_c = 7$AS in panels (c),(d), respectively. The local components are calculated at T=5K, 0.1 V bias, and $\theta = \pi/2$.

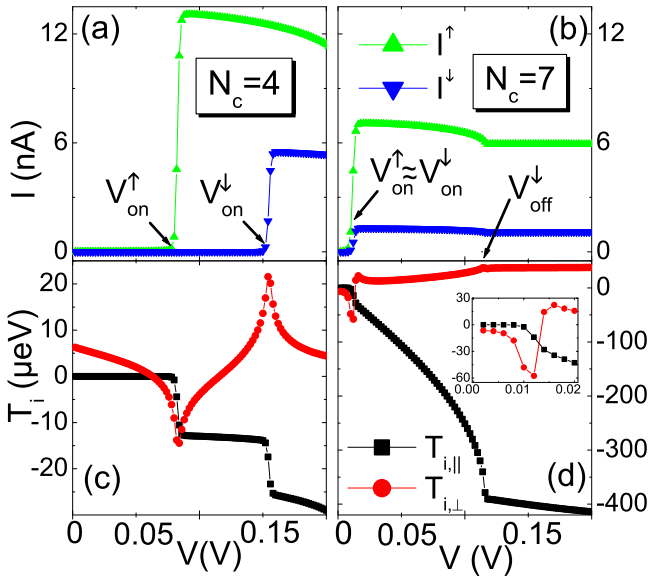

FIG. 6: (Color online) Low-temperature (T=5K) bias dependence of the majority (green symbols) and minority (blue symbols) currents in the central FM for (a) $N_c = 4$ AS and (b) $N_c = 7$AS, respectively, and for $\theta = \pi/2$. Bias dependence of $T_{i,||}$ (black symbols) and $T_{i,\perp}$ (red symbols) on the first site in the central FM, for (c) $N_c = 4$ AS and (d) $N_c = 7$. The bias $V^{\sigma}_{on(off)}$ denote the switch-on (-off) bias.

MTJ[3]. On the other hand, when the enhancement conditions are fulfilled for $N_c = 7$ AS (Fig. 4c), $T_{i,\perp}$ exhibits a non-sinusoidal angular dependence changing sign in the $[0, \pi]$ interval.

In Figs. 5(a),(c) and 5(b),(d) we display the perpendicular, $T_{i,\perp}$, (black squares) and parallel $T_{i,||}$ (red circles) components of the *local* spin torque as a function of site i in the central FM, for $N_c = 4$AS and $N_c = 7$AS, respectively. The spin torques are evaluated at T=5K, V=0.1V, and $\theta = \pi/2$. Interestingly both $T_{i,\perp}$ and $T_{i,||}$ oscillate around zero as function of atomic site i due to the electron precession in the central FM. The number of nodes increases as the width of the FM quantum well increases. The enhancement of $T_{i,\perp}$ and $T_{i,||}$ for $N_c = 7$ AS holds for all sites i.

In Figs. 6a and 6b, we display the low-temperature ($T = 5K$) bias dependence of the spin-polarized currents, $I^{\uparrow}$ and $I^{\downarrow}$, for $N_c = 4$AS and $N_c = 7$AS, respectively, and for $\theta = \frac{\pi}{2}$. The spin-polarized currents switch on at $V^{\sigma}_{on} = 2|E^{n\sigma} - E_F|$, when the n_σ QWS enters the bias energy window. For $N_c = 7$AS, the switch on for both spin-polarized currents occur at about the same bias, $V^{\uparrow}_{on} \approx V^{\downarrow}_{on}$, due to the fact that $|E^{1^{\downarrow}} - E_F| \approx |E^{3^{\uparrow}} - E_F|$ in Fig. 2. Both currents decrease with increasing bias because the density of states of the minority band in the leads at $E^{n^{\sigma}}$ decreases. At the critical bias, $V^{\downarrow}_{off} = 2(E^{n^{\sigma}} + |E^{\downarrow}_B|)$, the QWS energies, $E^{1^{\downarrow}}$ and $E^{3^{\uparrow}}$ are shifted below the bottom of the minority band of the lead, and hence the minority contribution to the spin-polarized currents is switched off.

In Figs. 6c and 6d we display the low-temperature ($T = 5K$) bias behavior of the parallel, $T_{i,||}$, (black squares) and perpendicular $T_{i,\perp}$ (red circles) components of the *local* spin torque on the first site in the central FM, for $\theta = \frac{\pi}{2}$ and for $N_c = 4$AS and $N_c = 7$AS, respectively. The local spin-transfer component, $T_{i,||}$, exhibits a switch on bias behavior at $V^{\uparrow}_{on}$ and at $V^{\downarrow}_{on}$, similar to that of the spin polarized currents in 6a. On the other hand, $T_{i,\perp}$, which is non-zero for zero bias, displays a non-monotonic bias dependence, changing sign between $V^{\uparrow}_{on}$ and $V^{\downarrow}_{on}$, similar to that of the exchange field in quantum dots connected to FM leads[22]. It is important to note that both $T_{i,||}$ and $T_{i,\perp}$ are strongly enhanced for $N_c = 7$AS in Fig. 6d, even though the corresponding spin-polarized currents are *smaller* than those for $N_c = 4$ AS. Thus, the enhancement of the local spin torque is not associated with a corresponding enhancement of the spin-polarized currents. This result clearly demonstrates that the underlying mechanism that controls the *local* spin-transfer torque *enhancement* is the close proximity of the majority and minority QWS energies of different quantum number, $E^{n^{\uparrow}} \approx E^{n'^{\downarrow}}$, within the bias energy window. This in turn enhances the spin mixing $\sigma \leftrightarrow \bar{\sigma}$ in the central FM, when electrons tunnel resonantly through the SPQWS. The enhancement of the local spin-transfer torque is independent of the parity of the QWS wavefunctions. This spin-transfer torque enhancement may have technological applications since the CIMS may be facilitated under such conditions.

In order to elucidate the role of the SPQWS on the enhancement and bias dependence of the local spin torque,

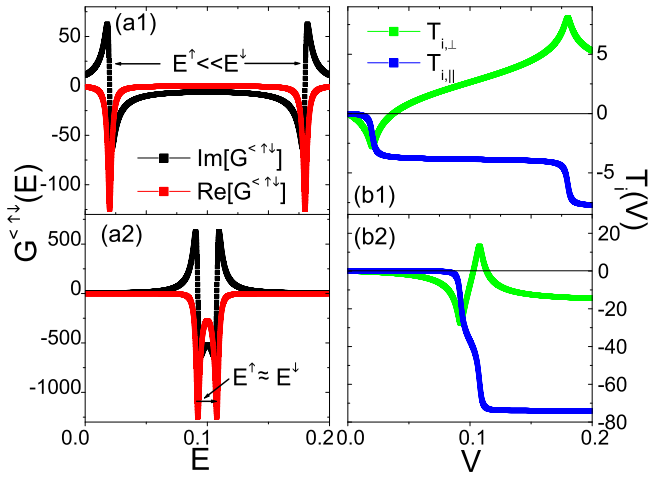

FIG. 7: (Color Online)(a1),(a2) Energy dependence of the real (red squares) and imaginary (black squares) parts of $G^{<\uparrow\downarrow}$ for ($E^{\uparrow} << E^{\uparrow}$) and ($E^{\uparrow} \approx E^{\uparrow}$), respectively;(b1) and (b2) bias dependence of $T_{i,||}$ (blue squares) and of $T_{i,\perp}$ (green squares) corresponding to (a1) and (a2), respectively.

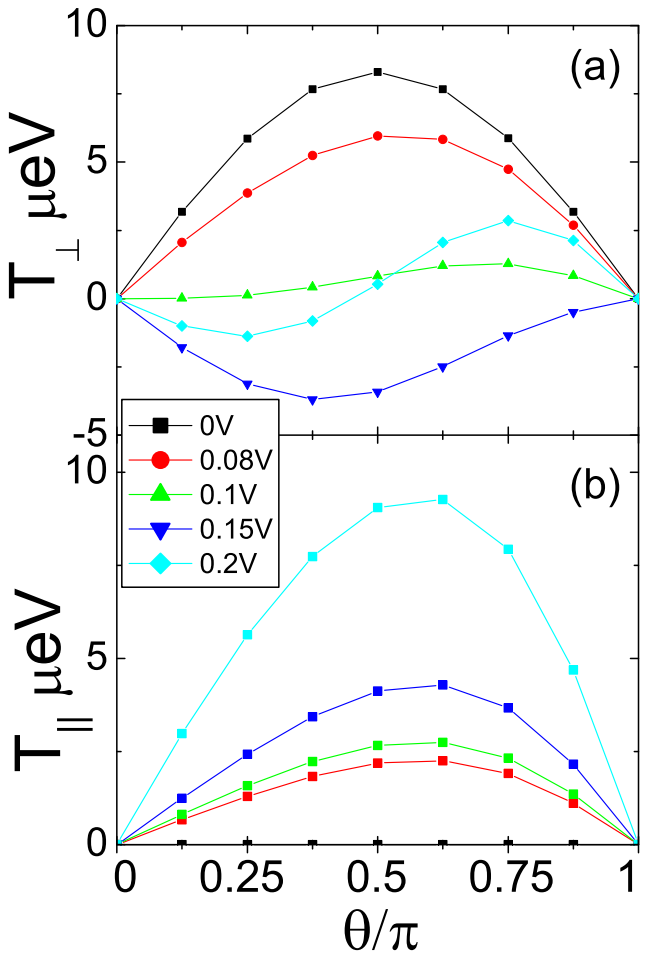

FIG. 8: (Color Online)(a) Angular dependence of the *net* (a) field-like torque and (b) spin-transfer torque, for $N_c = 4$ and various values of bias.

we have used a simple model of a central FM region consisting of a single-site coupled weakly to the leads. We have shown that to leading order in the coupling parameter, t_C, the on-site spin off-diagonal non-equilibrium Greens function is

$$G^{<\uparrow\downarrow} \approx i \sum_{\alpha=L,R} f_\alpha G_r^{\uparrow\uparrow} \Sigma_\alpha^{\uparrow\downarrow} G_a^{\downarrow\downarrow}. \quad (11)$$

Here, $\Sigma_\alpha^{\uparrow\downarrow} = t_C^2 \pi [N_\alpha^{\uparrow} - N_\alpha^{\downarrow}] sin(\theta)$ is the self-energy due to the leads, $N_\alpha^{\uparrow(\downarrow)}$ is the surface density of states of the L(R) leads, which for simplicity are taken to be energy independent. In the weak coupling regime, the retarded (advanced) Greens functions of the coupled system, $G_{r(a)}^{\sigma\sigma}$, can be be approximated with those of the uncoupled system $g_{r(a)}^{\sigma\sigma}$, i.e. $G_{r(a)}^{\sigma\sigma} \approx g_{r(a)}^{\sigma\sigma} = [E - E^{\sigma} \pm i\eta]^{-1}$, where η is taken to be spin-independent. Therefore, the spin-transfer torque components, determined by the non-equilibrium on-site magnetization [21], are

$$T_{i,||} \propto \int_{-\infty}^{eV} \frac{\eta(E^{\uparrow} - E^{\downarrow})}{((E - E^{\uparrow})^2 + \eta^2)((E - E^{\downarrow})^2 + \eta^2)} dE, \quad (12)$$

and

$$T_{i,\perp} \propto \int_{-\infty}^{eV} \frac{(E - E^{\uparrow})(E - E^{\downarrow}) + \eta^2}{((E - E^{\uparrow})^2 + \eta^2)((E - E^{\downarrow})^2 + \eta^2)} dE. \quad (13)$$

The energy dependence of the real (red squares) and imaginary (black squares) parts of $G^{<\uparrow\downarrow}$ for ($E^{\uparrow} << E^{\uparrow}$) and ($E^{\uparrow} \approx E^{\uparrow}$) are shown in panels (a1) and (a2) of Fig. 7, respectively. The corresponding bias dependence of $T_{i,||}$ (blue squares) and of $T_{i,\perp}$ (green squares) are shown in panels (b1) and (b2) of Fig. 7, respectively. One can clearly see that the overall bias dependence of this simple model reproduces qualitatively that displayed in Figs.6c and 6d. More specifically, the switch-on behavior for $T_{i,||}$ and the sign change of $T_{i,\perp}$ with bias are associated with the relative position of the majority and minority QWS energies which lie within the bias energy window. When $E^{\uparrow} \approx E^{\downarrow}$, both components of the spin-transfer torque are dramatically enhanced, as shown in Fig. 7(a2), due to the presence of higher-order poles in Eqs. (12) and (13).

The *net* spin torque components $T_{||(\perp)} = \sum_{i\varepsilon C} T_{i,||(\perp)}$, are not as strongly enhanced as the local torques, $T_{i,||}$ and $T_{i,\perp}$, which oscillate as a function of site i, due to the electron precession in the central FM (Fig.5). The angular dependence of the *net* field-like torque, $T_\perp$, and the spin-transfer torque $T_{||}$, is shown in Fig. 8a and 8b, respectively, for $N_c = 4$ AS and for various bias values. For zero bias $T_\perp$ displays sinusoidal behavior, which however, can change dramatically upon increasing the bias. The *net* field-like torque can be expressed[2, 24] as

$$T_\perp = -\partial E_{XC}(\theta)/\partial\theta, \quad (14)$$

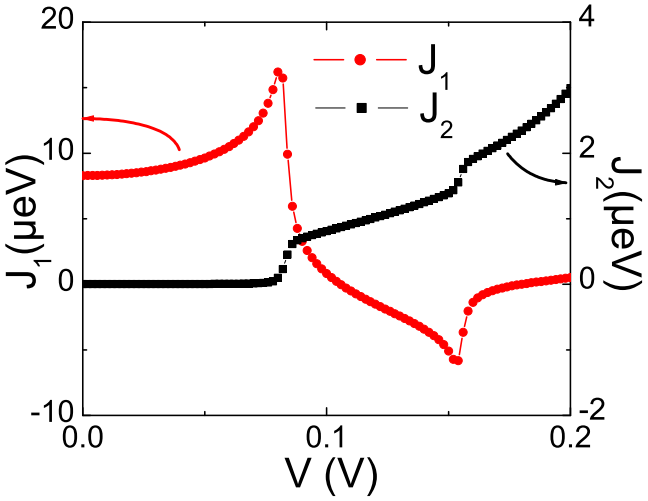

FIG. 9: (Color Online) Bias dependence of the non-equilibrium effective bilinear, J_1, and biquadratic, J_2, interlayer exchange couplings for $N_c = 4$.

where

$$E_{XC}(\theta) = -J_1 cos(\theta) - J_2 cos^2(\theta) + \ldots, \qquad (15)$$

is the *effective* exchange coupling energy [25], between $\mathbf{M}_C$ and $\mathbf{M}_{L(R)}$. The out of equilibrium interlayer exchange coupling has terms related to the spin-polarized tunnel current that can dominate and alter the coupling behavior under certain bias conditions[26]. Here, J_1 and J_2 are the *non equilibrium* bilinear and biquadratic effective exchange couplings, respectively, which are determined by fitting the angular dependence of $T_\perp(\theta)$ in Fig. 8 to the above expression for various biases. In Fig. 9 we show the bias dependence of J_1 and J_2 for $N_c = 4$ AS. It is important to note that J_1 (red circles) reverses its sign with bias, similar to $T_{i,\perp}(V)$ in Fig. 6c. On the other hand, the bias dependence of J_2 (black squares) exhibits the switch on bias behavior found for $T_{i,||}(V)$. Hence, there is a range of bias where $J_2 > J_1$, favoring perpendicular alignment of $\mathbf{M}_C$ and $\mathbf{M}_{L(R)}$[25]. In contrast, the angular dependence of the *net* $T_{||}$ exhibits a skewed sinusoidal behavior (8b) for any bias, similar to that found in spin valves.

IV. CONCLUSION

In summary, we demonstrate that the local spin-transfer torque can be dramatically enhanced, when the majority and minority QWS of different quantum number are in close energetic proximity and lie within the bias energy window. This enhancement may in turn lead to reduction of the critical current necessary for CIMS in magnetic memories. The spin-torque enhancement criterion may be achieved by controlling the SPQWS through an external magnetic field or spin-dependent barriers. The SPQWS tune selectively the bias dependence of the spin-transfer and field-like components of the *local* and the *net* spin torque. This results to an anomalous angular behavior of $T_\perp$ due to the bias interplay of the bilinear and biquadratic effective exchange couplings. Future work will be aimed to include the results for the local spin torques of these calculations as an input into the Landau-Lifshitz-Gilbert equation, to calculate the critical current for the CIMS.

V. ACKNOWLEDGEMENTS

The research was supported by NSF-PREM grant DMR-0611562, US Army grant W911NF-04-1-0058, and NSF-KITP grant PHY99-07949.

[1] I. Zŭtic , J. Fabian, S. Das Sarma, Rev. Mod. Phys. **76**, 323 (2004).
[2] J.C. Slonczewski, Phys. Rev. B **39**, 6995 (1989);
[3] J.C. Slonczewski, J. Magn. Magn. Mat. **159**, L1 (1996).
[4] L. Berger, Phys. Rev. B **54**, 9353 (1996).
[5] S. Zhang, P.M. Levy and A. Fert, Phys. Rev. Lett. **88**, 236601 (2002).
[6] M.D. Stiles and J. Miltat, in *Spin Dynamics in Confined Magnetic Structures III*(Springer, Berlin, 2006) p. 225.
[7] A. A. Tulapurkar, Y. Suzuki, A. Fukushima, H. Kubota, H. Maehara, K. Tsunekawa, D. D. Djayaprawira, N. Watanabe, and S. Yuasa, Nature (London) **438**, 339 (2005).
[8] J. C. Sankey, , P. M. Braganca, A. G. F. Garcia, I. N. Krivorotov, R. A. Buhrman, and D. C. Ralph, Phys. Rev. Lett. **96**, 227601, (2006).
[9] G. D. Fuchs, J. A. Katine, S. I. Kiselev, D. Mauri, K. S. Wooley, D. C. Ralph, and R. A. Buhrman, Phys. Rev. Lett. **96**, 186603 (2006).
[10] S. Urazhdin, H. Kurt, M. AlHajDarwish, Norman O. Birge, W. P. Pratt, Jr., and J. Bass, J. Appl. Phys. **97**, 10C701 (2005).
[11] Y. Huai, F. J. Albert, P. Nguyen, M. Pakala, and T. Valet, Appl. Phys. Lett., **84**, 3118 (2004).
[12] M. Hosomi *et al.* in *Electron Devices Meeting* (IEEE International, 2005) p. 459.
[13] A. G. Petukhov, A. N. Chantis, and D. O. Demchenko, Phys. Rev. Lett. **89**, 107205 (2002).
[14] Z.-Y. Lu, X.-G. Zhang, and S.T. Pantelides, Phys. Rev. Lett. **94**, 207210 (2005).
[15] Z.-M. Zeng, X.-F. Han, W.-S. Zhan, Y. Wang, Z. Zhang, and S.Zhang, Phys. Rev. B **72**, 054419 (2005).
[16] T. Nozaki, N. Tezuka, and K. Inomata, Phys. Rev. Lett. **96**, 027208 (2006) .
[17] K. Yakushiji, F. Ernult, H. Imamura, K. Yamane, S. Mitani, K. Takanashi, S. Takahashi, S. Maekawa and H.

Fujimori, Nat. Matter. **4**, 57 (2005).
[18] J. Hong, R.Q. Wu, R.B. Muniz, J. Magn. Magn. Mater. **270**, 298 (2004).
[19] S. Datta, *Electronic Transport in Mesoscopic Systems* (Cambridge University Press, Cambridge, 1995).
[20] I. Theodonis, Nicholas Kioussis, Alan Kalitsov, Mairbek Chshiev, and W. H. Butler, Phys. Rev. Lett. **97**, 237205 (2006).
[21] A. Kalitsov, I. Theodonis, N. Kioussis, M. Chshiev, W. H. Butler, A. Vedyayev, J. Appl. Phys. **99**, 08G501 (2006).
[22] M. Braun, J. Kŏnig and J. Martinek, Phys. Rev. B **70**, 195345 (2004).
[23] S. O. Demokritov J. Phys.D: Appl. Phys. **31** 925 (1998).
[24] J. d'Albuquerque e Castro , M.S. Ferreira, and R. B. Muniz Phys. Rev. B, **49**, 16062 (1994).
[25] J. C. Slonczewski J. Appl. Phys. **73**, 105957 (1993);J. Magn. Magn. Mater. **150**, 13 (1995).
[26] C. Heide, R. J. Elliot, and N. S. Wingreen, Phys. Rev. B **59**, 4287 (1999); C-Y You, and S. D. Bader, J. Magn. Magn. Mater. **195**, 488 (1999).